Far-infrared reflectivity spectroscopy of cuprous chloride, cuprous bromide and their mixed crystals

2000 J. Phys.: Condens. Matter 12 3461

(http://iopscience.iop.org/0953-8984/12/14/321)

J. Phys.: Condens. Matter **12** (2000) 3461–3484. Printed in the UK PII: S0953-8984(00)08079-6

Far-infrared reflectivity spectroscopy of cuprous chloride, cuprous bromide and their mixed crystals

Bruneau Wyncke and François Bréhat

Equipe Infrarouge, Université Henri Poincaré, Nancy 1, BP 239, 54506 Vandoeuvre lès Nancy Cédex, France

Received 23 September 1999, in final form 14 January 2000

Abstract. The temperature dependence of the far-infrared reflectivity spectrum of CuCl, CuBr and $CuCl_{1-x}Br_x$, in the zinc-blende structure, is reported over a wide temperature range (10–300 K). The analysis of the experimental data proves the activity of two polar lattice modes in both CuCl and CuBr: the expected lattice mode labelled γ and an additional lattice mode labelled β. The present work displays, for the first time, the activity of three lattice modes in the far-infrared reflectivity spectrum of $CuCl_{1-x}Br_x$, from room temperature down to liquid helium temperature. Side-bands due to two-phonon processes are observed in the low-frequency range of the reflectivity spectrum of both pure and mixed crystals. The phonon anomalies observed in both pure and mixed crystals are discussed and explained in agreement with the off-centre model.

1. Introduction

Cuprous halides have received much attention because many physical properties of these materials are of special interest. Cu halides exhibit an ionic conductive phase at high temperature, but at a low enough temperature they crystallize in the zinc-blende structure which is a non-conductive phase (γ phase). In this phase, a variety of anomalies are known to exist and they are especially pronounced in the phonon spectrum of both pure and mixed cuprous halides, whose lattice dynamical properties have been extensively studied for many years by infrared (IR) spectroscopy [1–6], Raman spectroscopy [7–24] and neutron scattering [25–30], from room temperature down to liquid helium temperature.

The zinc-blende structure of cuprous halides (T_d^2, $F\bar{4}3m$) contains two atoms in the primitive cell, therefore group theory predicts the activity of only one triply degenerate fundamental optical mode belonging to the Γ_{15} symmetry, which is Raman and IR active. This mode, labelled γ [10], is split into a transverse (TO) and longitudinal (LO) mode in the Raman spectrum. Early Raman measurements on CuCl indicated only the TO(γ) and LO(γ) mode [7], but later Raman experiments showed four peaks [8], displaying the activity of an additional lattice mode, observed also by IR spectroscopy [2]. This additional mode, labelled β [10], which is obviously a polar mode, has been observed in CuCl by Raman scattering [24], IR absorption [2–5] and reflection [2, 6] as well as neutron scattering [29, 30], from room temperature down to liquid helium temperature (see [20] and [24] for extensive references).

However, the temperature dependence study of the Raman spectra of CuCl, CuBr and CuI in the zinc-blende structure [22] has shown that while the two lattice modes γ and β are active at all temperatures in CuCl, the mode assigned to the β CuBr mode disappears below 80 K, while in CuI just the γ mode is active at temperature lower than 300 K. Similar results

0953-8984/00/143461+24$30.00

were obtained by IR reflectivity spectroscopy for CuCl and CuI [2, 6], while for CuBr only one mode was observed in the IR reflectivity and transmissivity spectra from 300 K down to 2 K [2, 6].

The main phonon anomaly in CuCl, i.e. the β and γ phonon mode activity observed in the IR [2, 3, 6] and Raman spectra [8–24], was successfully explained by using the off-centre model proposed by Vardeny and Brafman [20, 24]. This model is a modification of a disorder model [31] used to explain the unusually high values observed for the cation mean-square displacement, down to quite low temperatures: about 5 K in CuCl [32] and 150 K in CuBr [33]. The disorder model assumes that the copper may occupy one of four equivalent off-centre sites located on the [111] direction toward the faces of the tetrahedron formed by the anions, in addition to its ideal lattice site [31]. The off-centre model assumes also that the anharmonicity of the Cu halides is so high as to generate the four secondary off-centre minima in the Cu^+ cation potential energy, and introduces two hypotheses [20].

(a) A cation may occupy its ideal position as well as the four equivalent off-centre sites, the relative population of the off-centre sites depends only on the potential energy difference Δ of the respective well minima. To first approximation Δ is a function of temperature which affects the lattice constant and through that the relative off–on population.

(b) The off-centre model is a dynamical model in which the cation may tunnel among all five wells, and assuming that the tunnelling rate between central and off-centre sites is much lower than among the displaced sites, one may define two different sublattices: one with Cu^+ in the ideal sites, and the other with Cu^+ in the tunnelling off-centre states, both having the same T_d symmetry. The cations at off-centre sites would give rise to the β phonon mode, while in the γ phonon mode the cations in the ideal positions participate [20, 24].

Using the off-centre model, the explicit form of the cation potential in CuCl was calculated in terms of the Cu^+ displacement from its ideal site along the [111] direction ([24], section V B). The parameters used in the fit of the cation potential, the β and γ phonon frequencies and the activation energy Δ at different temperatures and pressures, were chosen such as to lead to a potential with two minima, with a potential-energy difference Δ between them equal to the values calculated assuming that the relative off-on population is proportional to the ratio of the two β, γ oscillator strengths: S_β/S_γ, obtained from polariton dispersion measurements ([24], figures 7(a) and 9), and with second derivatives in each minimum yielding the calculated ω_{on} and ω_{off} phonon frequencies ([24], figure 7(a)). These calculations show that the off-centre model may account quantitatively for the phonon anomaly in CuCl [24].

More recently, a theoretical study of the conditions for the occurrence of spontaneous off-centre atomic displacements in pure zinc-blende semiconductors has predicted that such instabilities will occur in the IB–VII and IIB–VI semiconductors, e.g. CuCl and CuBr [34]. The change in total energy was calculated for CuCl, CuBr and CuI, as a function of the [111] Cu^+ atomic displacement Q. The calculation leads in CuCl and CuBr to an overall minimum at the tetrahedra site ($Q = 0$), separated by a low-energy barrier E_b at Q_b from a second off-centre minimum at Q_0 at an energy Δ_0 above the global minimum ([34], figure 1). These calculations give theoretical support to the hypothesis that the additional β mode observed in CuCl could result from large cationic displacements [20, 24].

In addition to the phonon anomaly described above, a second phonon anomaly is observed in the Raman spectra of pure and mixed Cu halides: the activity of weak low-frequency Raman lines, which were assigned to disorder-induced first-order TA phonons [8, 12, 14, 20, 21]. Such side-bands have been observed also by IR transmissivity spectroscopy on both sides of the intense absorption modes [3–5]. Recently, theoretical linear response calculations performed

for the ideal zinc-blende structure of CuCl have succeeded in calculating the frequency values of the zone centre γ-mode, and those at the high-symmetry points of the Brillouin zone, in agreement with previous Raman and neutron scattering experiments ([35], table 2).

In contrast to the numerous Raman scattering studies, there are only a few papers devoted to the study of the far-IR reflectivity spectra of pure Cu halides [2, 6]. The optical constants of CuCl, CuBr and CuI have been calculated by the Kramers–Kronig analysis of the experimental data [2, 6], while only the TO frequencies of the β and γ modes active in CuCl were determined by fitting the experimental spectra by using the damped-harmonic oscillator model [3]. The far-IR transmissivity spectra of CuCl and CuBr were also studied [2–5].

However, to the authors' knowledge, far-IR reflectivity spectroscopy was never used to study the $CuCl_{1-x}Br_x$ mixed crystals, and there exists only one paper displaying the far-IR absorption spectra of $CuCl_{1-x}Br_x$ thin films at 2 K [18]. Nevertheless, Raman scattering was used to investigate both the behaviour of the optical phonon modes of mixed Cu halides at low temperature [13, 18, 23] and the weak low-frequency Raman lines [21].

The aim of the present paper is to study the temperature and concentration dependence of the far-IR reflectivity spectrum of CuCl, CuBr and their mixed crystals $CuCl_{1-x}Br_x$, and to discuss the phonon anomalies observed in the phonon spectrum of the Cu halides: the activity of an additional lattice mode, the β mode, together with that of weak low-frequency modes, contrarily to group theory predictions. The experimental techniques are described in section 2. Results are analysed and discussed in section 3 for CuCl and CuBr crystals, and in section 4 for $CuCl_{1-x}Br_x$ mixed crystals. Low-frequency modes observed in the spectrum of both pure and mixed crystals are discussed in section 5. The conclusions are summarized in section 6.

2. Experiment

Reagent grade powders of CuCl and CuBr were purified and then used as starting materials for crystal preparation. Pure CuCl and CuBr crystals were grown by the Bridgman method, in a fused quartz crucible. $CuCl_{1-x}Br_x$ mixed crystals, with $x = 0.25$, 0.45, 0.50 and 0.75, were prepared by melting the appropriate mixture of the constituent materials, and then grown in a similar way as for the pure samples. A plane parallel plate was cut in the ingots of both pure CuCl, CuBr and $CuCl_{1-x}Br_x$ mixed crystals and then polished to optical quality. The size of the samples was 10 mm in diameter and 6 mm for the thickness.

IR reflectivity spectra of both pure CuCl, CuBr and $CuCl_{1-x}Br_x$ mixed crystals were recorded in the frequency range 10–600 cm^{-1}, between 10 and 300 K, using a repetitive grating spectrometer equipped with a gallium-doped germanium bolometer [36].

3. Infrared reflectivity spectra of pure CuCl and CuBr crystals

3.1. Experimental data and their analysis

The temperature dependence of the IR reflectivity spectra of pure CuCl and CuBr crystals is displayed in figures 1(a) and 1(b). The spectra drawn in figure 1 are limited to 250 cm^{-1} and 200 cm^{-1} respectively for CuCl and CuBr, since no reflection band is observed from these limits up to 600 cm^{-1}. The usual slow rise in reflectivity is observed for both crystals up to 600 cm^{-1}. It is clearly seen, by comparison of figures 1(a) and 1(b), that the highest-frequency reflection band in the CuBr spectra has an anomalously asymmetric profile, even at 10 K, whose asymmetry increases with temperature (figure 1(b)), while the highest-frequency reflection band is symmetric at every temperature in the CuCl spectra (figure 1(a)).

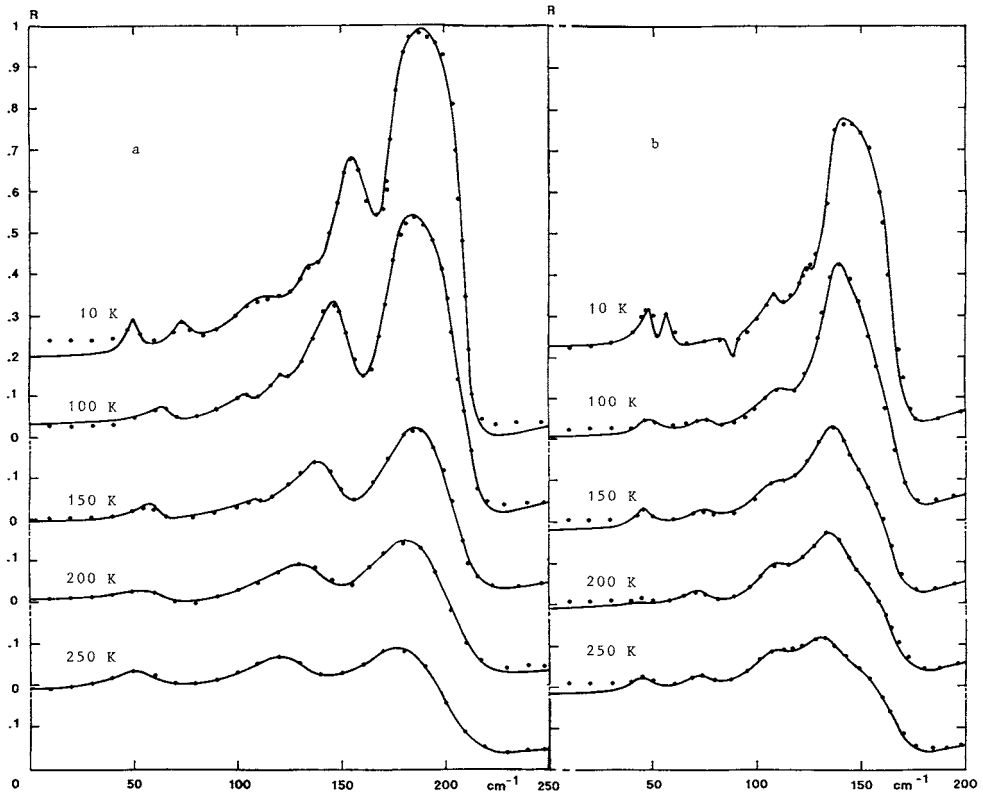

Figure 1. Temperature dependence of the CuCl (a) and CuBr (b) reflectivity spectrum. Full lines represent the best simulation of the experimental data to the factorized form of the dielectric function model. Dots represent the experimental data.

The IR reflectivity spectra of CuCl (figure 1(a)) are in good agreement with previous IR reflectivity studies [2, 6]: two main reflection bands are observed between 100 and 200 cm^{-1}, in the frequency range which corresponds to the lattice mode, from room temperature down to liquid helium temperature (figure 1(a)). While in the same frequency range, the measured reflectivity spectra of CuBr differ from those previously published [2, 6], e.g. at 250 K we observe clearly two reflectivity maxima at about 110 and 130 cm^{-1}, and an inflexion near 140 cm^{-1} (figure 1(b)), which were not observed in the pioneer work of Morlot and Hadni [2], who observed in CuBr only one reflection band, from room temperature down to liquid helium temperature [2]. The reflectivity of both CuCl and CuBr is strongly temperature dependent in the spectral range 100–200 cm^{-1} (figure 1), as previously observed [2]. In addition to the main reflection bands, several weak reflection bands are observed in the low-frequency range below 130 cm^{-1} for both CuCl and CuBr, which are more clearly observed at low temperature (figure 1).

The optical mode parameters, frequency Ω_j and damping γ_j for each transversal (TO) and longitudinal (LO) IR active phonon mode, were obtained from the simulation of the experimental reflectivity spectra $R(\omega)$ using the factorized form of the dielectric function [37]. Good fits were achieved in the whole frequency range (10–600 cm^{-1}), at each temperature for the two studied crystals, as shown in figure 1. The lattice mode parameters, frequency and damping, used in the fitting procedure are listed in tables 1 and 2, at three temperatures.

Table 1. Frequencies and dampings (in cm^{-1}) of the IR active modes of CuCl, deduced from the present IR reflectivity spectra.

10 K				150 K				250 K				
Ω_{TO}	γ_{TO}	Ω_{LO}	γ_{LO}	Ω_{TO}	γ_{TO}	Ω_{LO}	γ_{LO}	Ω_{TO}	γ_{TO}	Ω_{LO}	γ_{LO}	
50	5	50.1	7.2	53	9.5	53.8	9.5	50	21	51	27	
72	8.6	72.01	11.5									
109.4	22	110.7	32	105	6	105.05	6					
133	8.2	133.5	10.5									
151.4	8.4	165.3	18.5	140	25	150.9	25	122	30.5	129.8	39	β
173.6	9	210.8	5.5	176.2	24.4	212	24.4	174.9	43	207.9	40	γ

Table 2. As table 1 for CuBr.

10 K				150 K				250 K				
Ω_{TO}	γ_{TO}	Ω_{LO}	γ_{LO}	Ω_{TO}	γ_{TO}	Ω_{LO}	γ_{LO}	Ω_{TO}	γ_{TO}	Ω_{LO}	γ_{LO}	
48.2	5	49.5	7	46	8	46.15	10	44.9	11.1	45.4	13	
56.4	3.8	56.7	6	74	16	74.5	18	72.6	13	73.3	15	
88	4.8	88.1	3.5									
108.2	7.3	108.9	9.5	107	17.5	107.4	22.5	108	16.7	109.6	21.2	
124	4.5	124.5	5.1									
136.6	4.6	150.4	28	134	17	143.6	25	130.3	22	136.9	28	β
151	23	168.2	13.5	151	36.5	167.9	21	151	40.9	169	29.3	γ

Table 3. TO and LO frequencies (in cm^{-1}) determined by the Kramers–Kronig analysis of the IR reflectivity spectrum and by the direct observation of thin-film transmission spectra at normal and the oblique incidence at 2 K, for CuCl and CuBr, from Namba *et al* [6].

	Reflection analysis		Transmission	
	TO	LO	TO	LO
CuCl	173.3	209.5	173.5	209.7
	166.5		165	
	155.7		156	
CuBr	136	167	136	166

However, as pointed out above, the reflectivity profile of the main reflection band of the CuBr reflectivity spectra (110–170 cm^{-1}) is highly asymmetric, especially when temperature increases up to 250 K (figure 1(b)). Therefore two oscillators were used to fit the reflectivity spectra of CuBr above 130 cm^{-1} (table 2), in order to take into account the inflexion observed near 140 cm^{-1} in the experimental reflectivity curves (figure 1(b)). Then the agreement between the calculated curves and the experimental data is excellent since it is within the experimental errors (figure 1(b)). In tables 3 and 4 are listed the TO and LO lattice mode frequencies obtained from previous IR and Raman spectroscopic studies, for comparison with the present work [6, 22].

The temperature dependence of the TO and LO optical mode frequencies, deduced from the fitting procedure, is displayed in figures 2(a) and 2(b) for CuCl and CuBr respectively, from 300 down to 10 K. The oscillator strengths of the IR active modes, calculated from their

Table 4. Frequencies (in cm^{-1}) of the β and γ modes obtained from the polariton Raman spectra of CuCl and CuBr [22]. The frequency of the LO(β) mode in CuBr was calculated from the second zero of $\varepsilon(\omega)$ [22].

	CuCl				CuBr			
T (K)	TO(β)	LO(β)	TO(γ)	LO(γ)	TO(β)	LO(β)	TO(γ)	LO(γ)
2	155	166.5	174	208			140	169
80	149	161	173	210	121	(122.5)	138	169
300	123	139	162	202	114	(119)	124	163

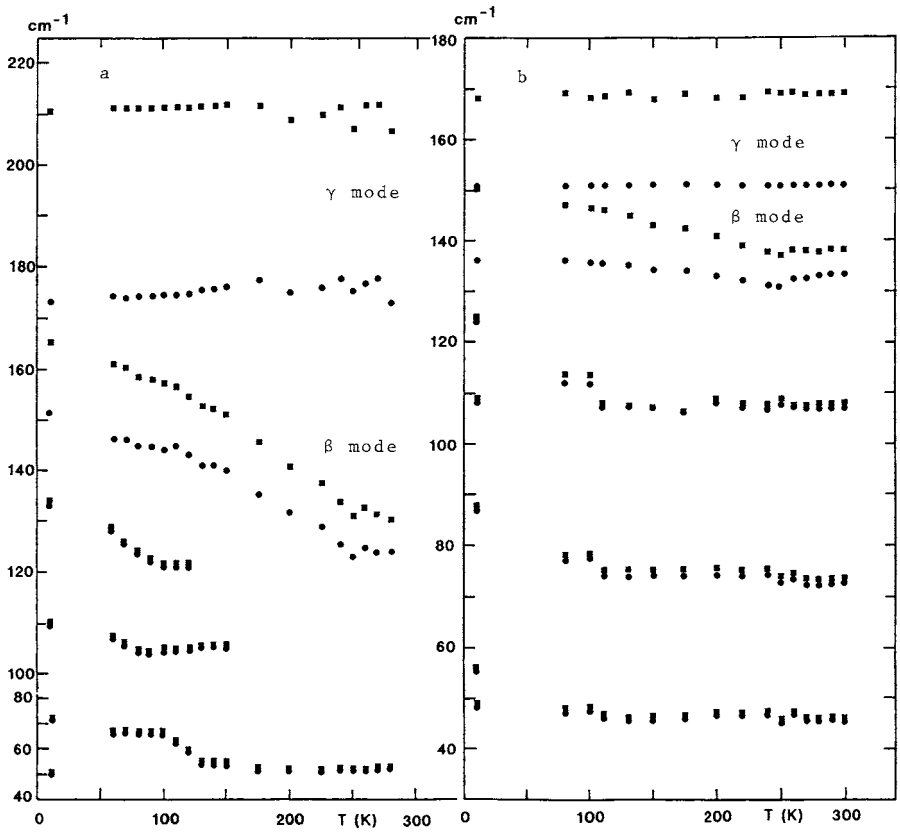

Figure 2. Temperature dependence of the TO (●) and LO (■) frequencies of CuCl (a) and CuBr (b).

TO and LO optical mode frequencies [37], are reported in tables 5 and 6 at 10 and 250 K. The temperature dependence of the TO oscillator strength of the two highest-frequency modes is displayed in figures 3(a) and 3(b), for CuCl and CuBr respectively.

3.2. Discussion

The analysis of the present IR reflectivity spectra of pure CuCl and CuBr crystals proves the activity of two polar lattice modes in the 100–250 cm^{-1} frequency range, at every temperature between 300 and 10 K, in both crystals: the expected lattice mode labelled γ together with

Table 5. Frequencies, dampings (in cm^{-1}) and TO oscillator strengths ($\Delta\varepsilon$) of the IR active modes in $CuCl_{1-x}Br_x$ mixed crystals, together with those of pure CuCl and CuBr, as functions of concentration x at 10 K.

	$x = 0$ (CuCl)					$x = 0.25$					$x = 0.45$					
	Ω_{TO}	γ_{TO}	Ω_{LO}	γ_{LO}	$\Delta\varepsilon$	Ω_{TO}	γ_{TO}	Ω_{LO}	γ_{LO}	$\Delta\varepsilon$	Ω_{TO}	γ_{TO}	Ω_{LO}	γ_{LO}	$\Delta\varepsilon$	
	50	5	50.1	7.2	0.028	58	7.7	59.3	8.3	0.395	53	5.9	54.7	10	0.542	
	72	8.6	72.01	11.5	0.002	77	3.8	77.5	4.4	0.112	76	2	76.3	2.3	0.066	
	109.4	22	110.7	32	0.195	108	6.5	108.3	6.5	0.065	108	5	108.6	5.2	0.128	
	133	8.2	133.5	10.5	0.088	130	8.8	131	7.8	0.331	127	6.1	127.3	5.2	0.091	
						141.5	5.4	151	10.4	2.26	139.5	8	150.7	14	2.304 osc. 1	
β	151.4	8.4	165.3	18.5	2.08	151	13	161	12.4	0.001	152.4	22.7	164.4	10	0.181 osc. 2	
γ	173.6	9	210.8	5.5	0.687	177	5.6	205	13.8	0.697	181	9.7	203.4	27.5	0.515 osc. 3	
	$x = 0.5$					$x = 0.75$					$x = 1$ (CuBr)					
	Ω_{TO}	γ_{TO}	Ω_{LO}	γ_{LO}	$\Delta\varepsilon$	Ω_{TO}	γ_{TO}	Ω_{LO}	γ_{LO}	$\Delta\varepsilon$	Ω_{TO}	γ_{TO}	Ω_{LO}	γ_{LO}	$\Delta\varepsilon$	
						48.2	5	49.1	5.5	0.318	48.2	5	49.5	7	0.448	
	58.3	5	59.6	11	0.396	56.5	4	56.8	6.5	0.08	56.4	3.8	56.7	6	0.096	
	74	2.8	74	3.2	0.001	78.5	4	79	4.4	0.116	88	4.8	88.1	3.5	0.061	
	108.6	5.9	109	6.9	0.095	106.8	8.9	110	11.5	0.687	108.2	7.3	108.9	9.5	0.142	
	124.9	9.3	125.7	11.1	0.246	119.7	10.7	120.5	21.7	0.156	124	4.5	124.5	5.1	0.134	
osc. 1	139	5.4	150.8	12.1	2.468	135.3	4.5	150.9	10	1.999	136.6	4.6	150.4	28	1.937	β
osc. 2	152.2	18.4	165.5	9.2	0.156	151	10	164.6	13.9	0.005	151	23	168.2	13.5	0.198	γ
osc. 3	183	9	203.5	25	0.477	187	12.7	191	25.8	0.093						
						216	17.7	218.3	14.8	0.054						

Table 6. As table 5 for 250 K.

	$x = 0$ (CuCl)					$x = 0.25$					$x = 0.45$					
	Ω_{TO}	γ_{TO}	Ω_{LO}	γ_{LO}	$\Delta\varepsilon$	Ω_{TO}	γ_{TO}	Ω_{LO}	γ_{LO}	$\Delta\varepsilon$	Ω_{TO}	γ_{TO}	Ω_{LO}	γ_{LO}	$\Delta\varepsilon$	
	50	21	51	27	0.24	58	23.5	62	29.5	0.882	48.1	8.4	48.9	10	0.238	
											70	13.9	71.8	15.4	0.355	
						95	14.2	95	15	0.001	99	17.2	99.4	18	0.068	
β	122	30.5	129.8	39	0.87	124	35	131.2	14	1.314	125.1	33.1	133.6	21.1	1.406 osc. 1	
						132.5	15	142.6	49	0.125	138.4	24.5	153.6	48.5	0.396 osc. 2	
γ	174.9	43	207.9	40	1.332	185.5	41	205	38.5	0.591	196.3	38.3	206.7	38	0.291 osc. 3	
	$x = 0.5$					$x = 0.75$					$x = 1$ (CuBr)					
	Ω_{TO}	γ_{TO}	Ω_{LO}	γ_{LO}	$\Delta\varepsilon$	Ω_{TO}	γ_{TO}	Ω_{LO}	γ_{LO}	$\Delta\varepsilon$	Ω_{TO}	γ_{TO}	Ω_{LO}	γ_{LO}	$\Delta\varepsilon$	
	55.4	23.8	58.6	28.5	0.734	49.6	8.5	50.6	10.2	0.277	44.9	11.1	45.4	13	0.146	
						63.9	14.6	64.7	17	0.158	72.6	13	73.3	15	0.132	
	99.3	17.2	100.2	18	0.143	106	11.9	106.4	13	0.069	108	16.7	109.6	21.2	0.254	
osc. 1	126	35	136	20	1.389	128	31	136	27	1.151	130.3	22	136.9	28	0.82	β
osc. 2	139	19	152	50	0.196	147.5	37	166	36	0.729	151	40.9	169	29.3	0.727	γ
osc. 3	195.2	31.4	203.6	32.3	0.225	199.3	32.4	207.2	37.6	0.192						

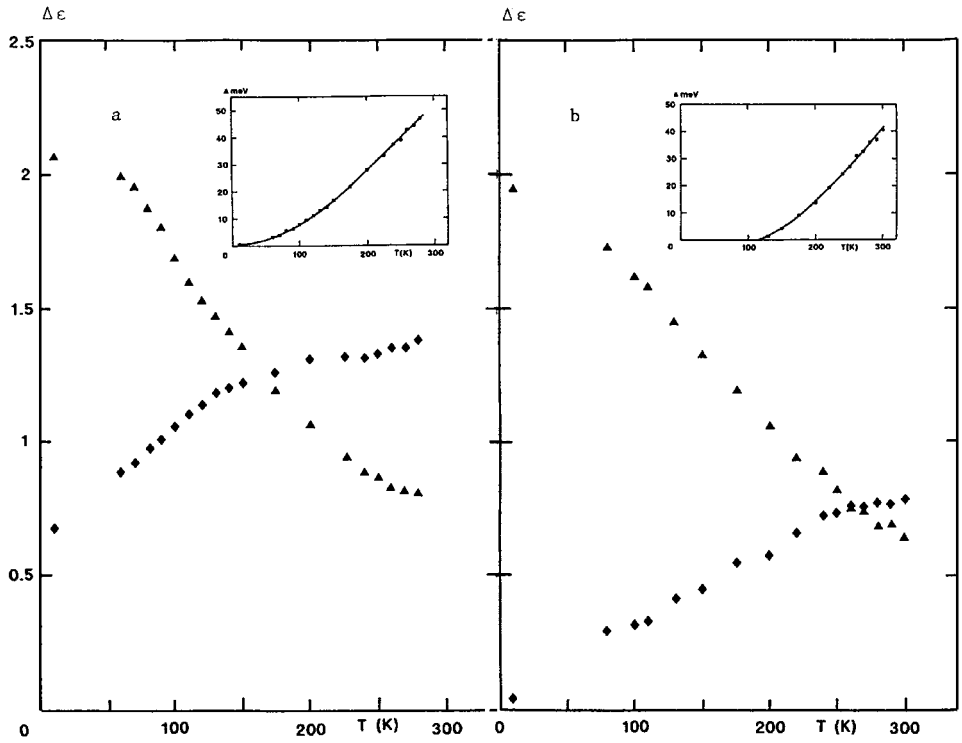

Figure 3. Temperature dependence of the oscillator strength ($\Delta\varepsilon$) of the β (▲) and γ (♦) mode of CuCl (a) and CuBr (b). Inset: temperature dependence of the activation energy Δ (see text section 3.2); the line serves as a guide to the eye.

an additional lattice mode labelled β, which are strongly affected by temperature variation (figures 1–3, tables 1 and 2).

For CuCl the present results are in good agreement not only with the previous far-IR spectroscopic measurements [1–6] (tables 1 and 3), but also with previous Raman studies [10–12, 14–17, 20, 22, 24]: the frequencies of the γ and β modes reported in table 4 are in good agreement with those of table 1, and the values of the oscillator strength of the Raman γ CuCl mode S_γ ([22], table I) are in agreement with the values of $\Delta\varepsilon_{\gamma(CuCl)}$ listed in tables 5 and 6. For CuBr, comparison of the results reported in table 2 with those reported in tables 3 and 4 shows that the TO frequency (TO_β) and the LO frequency of the γ mode (LO_γ), respectively 136.6 and 168.2 cm^{-1} at 10 K, agree very well with the TO and LO frequencies of the lattice mode observed in CuBr at 2 K by both IR reflectivity and absorption spectroscopy (table 3), as well as with those of the highest frequency mode observed in Raman spectroscopy and assigned to the γ mode in [22] (table 4). Our results seem to be in contradiction with these spectroscopic studies. Nevertheless, we were able to obtain a good fit to our experimental IR reflectivity spectra of CuBr below 100 K, by using only one lattice mode whose TO and LO frequencies are 136.6 and 169.1 cm^{-1} respectively at 10 K, in agreement with the values reported at 2 K from both IR reflectivity measurements (table 3) and Raman spectroscopy (table 4, mode labelled γ). The difference between the LO_β and TO_γ frequencies is very weak at 10 K, about 0.6 cm^{-1}, it remains lower than 4 cm^{-1} below 110 K and then increases with temperature up to 14 cm^{-1} at 250 K (table 2, figure 2(b)), together with the asymmetry of the

main reflection band (figure 1(b)). At temperatures higher than 100 K, it is no longer possible to fit the experimental asymmetric reflectivity spectra of CuBr with only one mode: two modes are needed (table 2).

The discrepancy between our results for CuBr (table 2) and those obtained from Raman spectroscopy (table 4) can be explained by a too weak Raman intensity of the two Raman lines corresponding to the IR LO_β and TO_γ modes (table 2), which prevents their observation in the Raman spectrum, and, therefore, only the most intense Raman lines are observed [22]. The phonon–polariton spectra of CuBr display the activity of only one polar mode labelled γ in [22], whose TO(γ) and LO(γ) frequencies are reported in table 4. At 250 K the oscillator strength S_γ ([22], table II) corresponds to the sum of the oscillator strength of the β and γ CuBr modes, $\Delta\varepsilon_\beta$ and $\Delta\varepsilon_\gamma$, calculated in the present work at the same temperature, and reported in table 6. In addition, the LO frequency corresponding to the TO line assigned to the TO(β) mode in [22] was never observed between 2 and 300 K, but it was calculated from the second zero of $\varepsilon(\omega)$ ([22], section III b). This mode cannot be the additional β mode of CuBr, as proposed in [22]. To support this explanation, it is to be noted that in CuCl the four Raman lines corresponding to the two polar β and γ modes were clearly reported only at 2 K [20, 22], while at 300 and 80 K only three Raman lines are observed: TO(β), TO(γ) and LO(γ) [20], and it was necessary to use the polariton measurements to prove the existence of the two polar β and γ modes in CuCl at 300 K and below ([22], section III B). Moreover, in CuCl at 2 K, the Raman intensity of both LO(β) and TO(γ) lines [20, 24], which correspond respectively to the LO_β and TO_γ frequencies of the IR active β and γ modes, not observed in the CuBr Raman spectra [22], is lower than the intensity of the two other lines TO(β) and LO(γ) of CuCl [20, 22, 24].

Nevertheless, the characteristic features observed in the present analysis of the CuCl and CuBr IR reflectivity spectra (figures 1–3) agree very well with those observed in the Raman study of CuCl crystal [24], and verify the hypotheses of the off-centre model [20, 24].

(i) The strong increase of the lattice mode damping (tables 1 and 2), corresponding to the strong decrease of the reflectivity level in the 100–200 cm^{-1} frequency range, with increasing temperature (figure 1), reveals the high degree of anharmonicity of both CuCl and CuBr crystals, as observed experimentally by structural investigations [31–33].

(ii) The TO and LO frequencies of the extra β mode are more sensitive to the increase of temperature than those of the γ mode: they decrease by about 30 cm^{-1} for CuCl and 15 cm^{-1} for CuBr when temperature increases from 10 up to 300 K, while those of the γ mode are nearly temperature independent (figure 2). The temperature variation of the β and γ mode frequencies of CuCl, displayed in figure 2(a), is in good agreement with that of the ω_{off} and ω_{on} frequencies, respectively, calculated from the theoretical expression for the cation potential using the experimental results of the polariton measurements ([24], figure 7(a)).

(iii) The temperature dependence of the oscillator strengths of the β and γ modes ($\Delta\varepsilon_\beta$ and $\Delta\varepsilon_\gamma$) is similar for CuCl and CuBr: $\Delta\varepsilon_\gamma$ increases while $\Delta\varepsilon_\beta$ decreases with temperature (figure 3). For CuCl, the values of $\Delta\varepsilon_\gamma$ (figure 3(a)) agree very well with the oscillator strengths of the γ mode (S_γ) obtained from the polariton measurements ([22], table I; [24], figure 6(b)), while we observe a constant decrease of $\Delta\varepsilon_\beta$ with increasing temperature (figure 3(a)), in contrast to the Raman study which indicates for S_β a decrease from 2 up to 100 K and then an increase with temperature above 100 K ([24], figure 6(b), [22], table I). For CuBr, the values $\Delta\varepsilon_\beta$ and $\Delta\varepsilon_\gamma$ do not correspond to the values S_β and S_γ obtained from polariton measurements, and reported in table II of [22] (see above).

(iv) The temperature dependence of the oscillator strength of the β and γ modes being known (figure 3), we have calculated the potential energy difference Δ by using the relation [24]

$$\frac{N_{off}}{N_{on}} = 4\exp\left(-\frac{\Delta}{kT}\right) \tag{1}$$

assuming that the relative off–on population N_{off}/N_{on} is proportional to the ratio of the two oscillator strengths $\Delta\varepsilon_\beta/\Delta\varepsilon_\gamma$. The values obtained for Δ are shown in the inset of figures 3(a) and 3(b), for CuCl and CuBr respectively. For CuCl these values agree very well in the temperature region 10–100 K, with both the experimental values obtained by Livescu and Brafman from their polariton measurements ([24], figure 6(a)), and the calculated ones from the theoretical expression for the cation potential ([24], figure 7(a)): Δ increases with temperature (figure 3(a)), according to the off-centre model [20]. One of the arguments in the model, to explain the existence of a second oscillator at very low temperature, is based on the negative thermal expansion coefficient of CuCl below 100 K [38], which means that the interatomic distances decrease when the temperature is raised. The off-centre Cu^+ potential well deepens at low temperatures [20], and consequently the off-centre Cu^+ population increases with decreasing temperature. This is manifested by the constant decrease of the term Δ/kT, from 1 at 110 K to about 0.3 at 10 K, reflected in the increase of $\Delta\varepsilon_\beta$ as seen in figure 3(a), in agreement with the results of [24]. Above 100 K, Δ keeps increasing with temperature (figure 3(a)), despite the positive thermal expansion coefficient [38], but in agreement with the decrease of $\Delta\varepsilon_\beta$ observed in figure 3(a). It is to be noted that Vardeny and Brafman [22] consider the fit they obtained at 300 K may be misleading, regarding the very broad lines of CuCl at this temperature ([22], section IV, figure 4), and therefore the value of the oscillator strengths deduced from the fit are more reliable at low temperature (< 100 K) than at higher temperature. We can trust the values of $\Delta\varepsilon_\beta$ we have obtained and reported as a function of the temperature in figure 3(a), since they are deduced from the fit of the far-IR reflectivity spectrum of CuCl, displaying two well separated reflection bands at all temperatures (figure 1(a)). Above 130 K, these values seem more reliable than those obtained from the polariton dispersion calculation [22]. The increase of Δ above 130 K can be explained by considering that the increase of the temperature affects not only the lattice parameter, but also the vibrational amplitudes of Cu^+ [32] and introduces anharmonicity in the CuCl lattice. Therefore, we can conclude, from the analysis of the experimental far-IR reflectivity spectra of CuCl, that the off-centre Cu^+ population keeps decreasing with increasing temperature above 130 K. The ratio $\Delta\varepsilon_\beta/\Delta\varepsilon_\gamma$ related to Δ through relation (1), which decreases from about three at 10 K to about 0.6 at 300 K, can be regarded as a measure of the ratio between the off-centre population and that of the centre, respectively.

The results displayed in figure 3(b) for CuBr are similar to those obtained for CuCl (figure 3(a)), and confirm the explanation given above. The only difference between the two crystals, that Δ increases with temperature from a zero value at 110 K (figure 3(b)), while for CuCl Δ begins to increase from zero above 10 K (figure 3(a)), can be related to the cation mean-square displacement, which has an anomalously high value down to 150 K in CuBr [33] and 5 K in CuCl [32].

4. Infrared reflectivity spectra of $CuCl_{1-x}Br_x$ mixed crystals

4.1. Experimental data and their analysis

The concentration dependence of the far-IR reflectivity spectra of $CuCl_{1-x}Br_x$ mixed crystals is displayed in figure 4 for 10 K; their temperature dependence is displayed in figure 5. The spectra

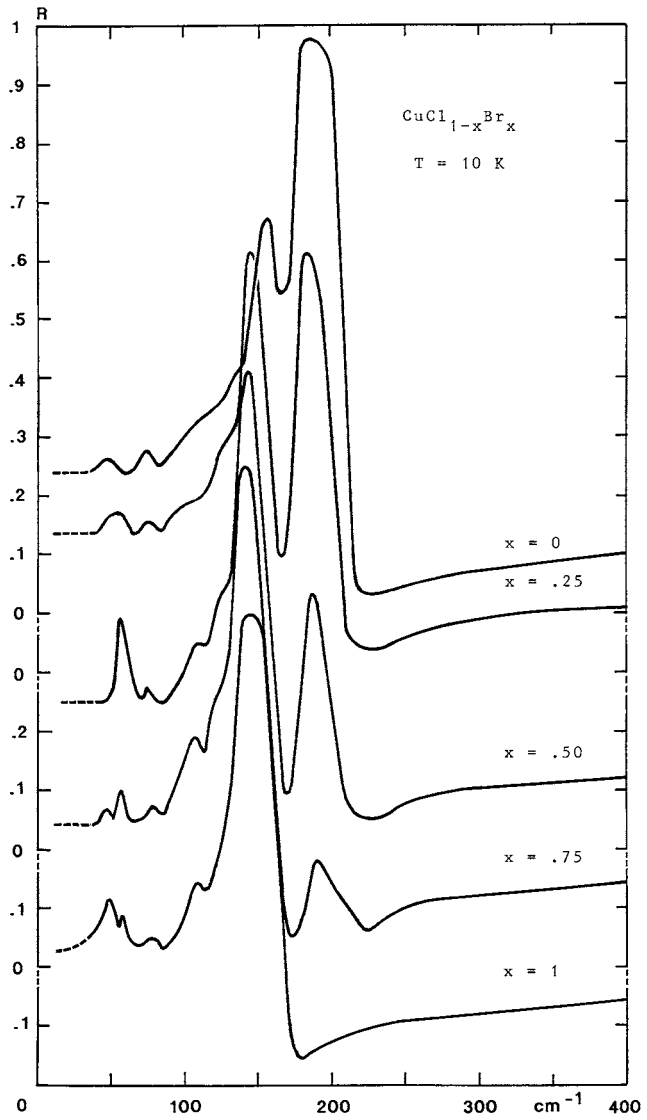

Figure 4. Experimental IR reflectivity spectra of $CuCl_{1-x}Br_x$ mixed crystals at 10 K.

drawn in figure 5 are limited at 300 cm^{-1}, since any reflection band is observed from this limit up to 600 cm^{-1}, as in pure CuCl and CuBr crystals (section 3.1). Inspection of figures 4 and 5 shows that the far-IR reflectivity spectrum of $CuCl_{1-x}Br_x$ mixed crystals can be divided into two parts, as observed in pure compounds (section 3, figure 1): the low-frequency range below 130 cm^{-1} in which weak reflection bands are observed, and the high-frequency range above 130 cm^{-1} in which two main reflection bands appear in each spectrum for $0 < x < 1$ (figure 4). The reflectivity of all the studied mixed Cu halide crystals is strongly temperature dependent in the frequency range 100–200 cm^{-1} (figure 5), as observed in the case of pure compounds.

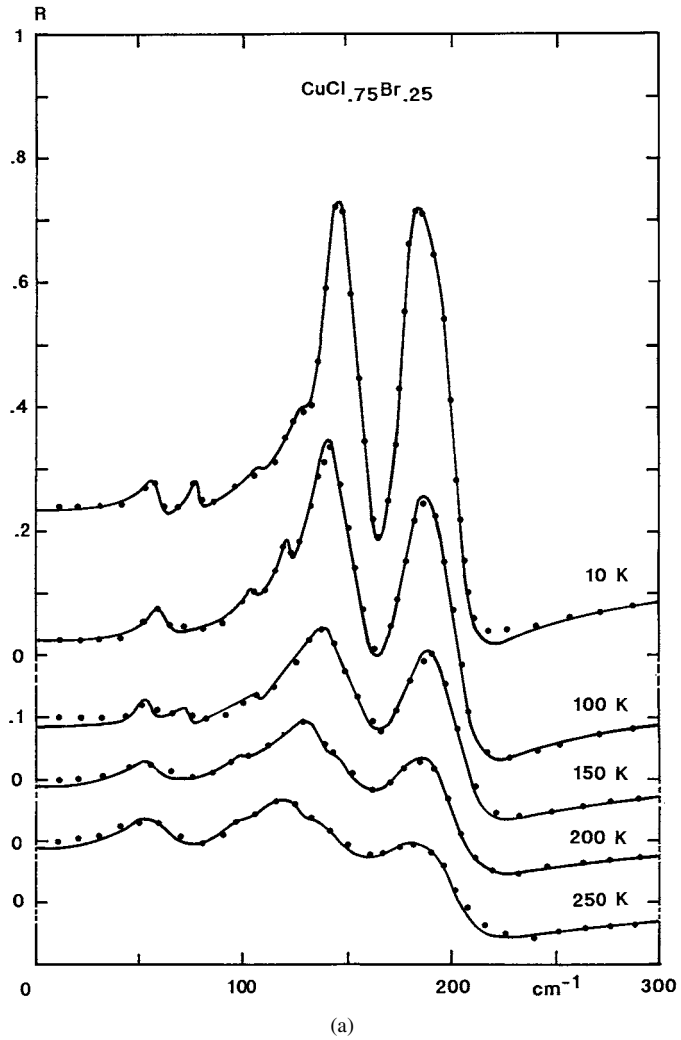

(a)

Figure 5. Temperature dependence of $CuCl_{1-x}Br_x$ mixed crystal reflectivity spectra. Full lines represent the best simulation of the experimental data to the factorized form of the dielectric function model. Dots represent the experimental data: (a) for $x = 0.25$; (b) for $x = 0.5$; (c) for $x = 0.75$.

The highest-frequency reflection band observed in figure 4, above 175 cm^{-1}, is clearly due to CuCl: its intensity decreases with x increasing from zero and it disappears for $x = 1$. The second strongest reflection band is observed in each spectrum for $0 \leqslant x \leqslant 1$ in the frequency range 130–170 cm^{-1} (figure 4), where both pure CuCl and CuBr crystals display a characteristic reflection band (figure 1) (tables 1 and 2), and therefore it arises from the contribution of the two constituents. Inspection of figure 5 shows an inflexion near 130 cm^{-1} in the high-frequency part of this reflection band, giving it an asymmetric profile.

The experimental reflectivity spectra of $CuCl_{1-x}Br_x$ mixed crystals (10–600 cm^{-1}) have been fitted to the factorized form of the dielectric function model (section 3.1). Good fits were achieved for each spectrum in the whole frequency range, as shown in figure 5, by using three oscillators labelled 1, 2 and 3 (tables 5 and 6) in the spectral range 130–250 cm^{-1} in which the

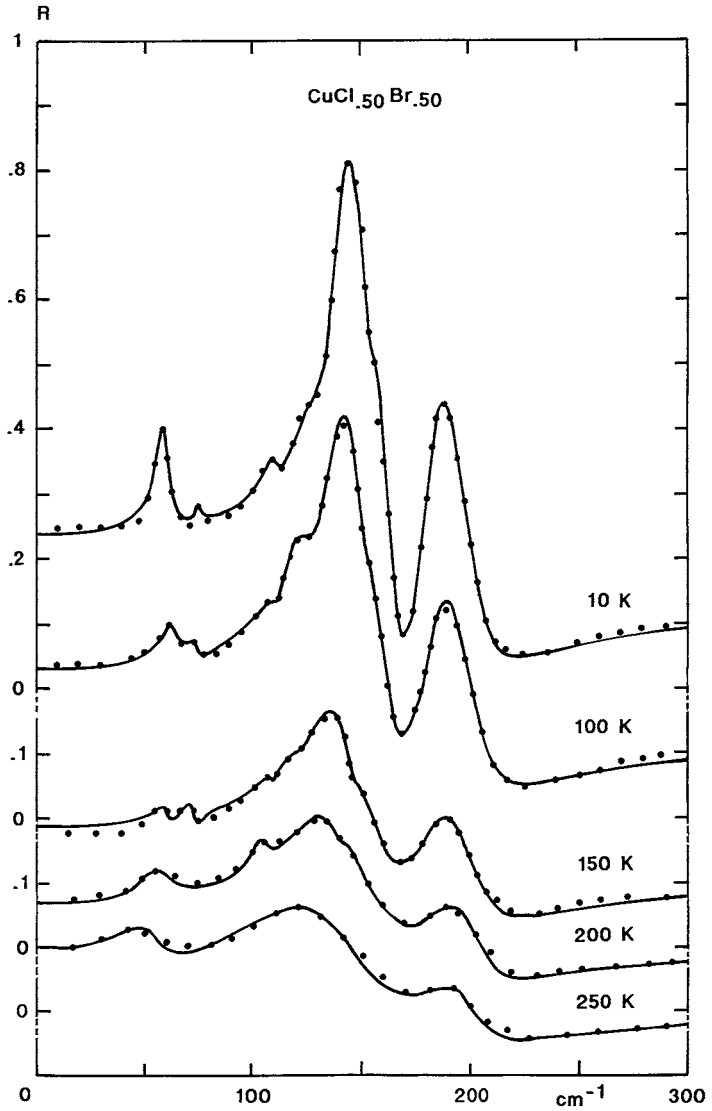

(b)

Figure 5. (Continued)

two main reflection bands are observed: oscillators 1 and 2 were used to fit the asymmetric reflection band (130–170 cm^{-1}) and oscillator 3 for the highest-frequency reflection band (170–230 cm^{-1}). The optical mode parameters, frequency and damping, deduced from the fitting procedure at 10 and 250 K, together with the oscillator strength of the IR active modes, are listed respectively in tables 5 and 6. The concentration dependence of the TO and LO optical mode frequencies is displayed in figure 6. Their temperature dependence is displayed in figure 7, which shows that the TO and LO frequencies of oscillators 1 and 2 are more sensitive to the increase of temperature for low than for high concentrations. For $x < 0.5$, the TO and LO frequencies of both oscillators 1 and 2 decrease strongly with increasing temperature (figure 7), as do those of the CuCl β mode (figure 2(a)) (tables 5 and 6). For $x > 0.5$, the frequencies

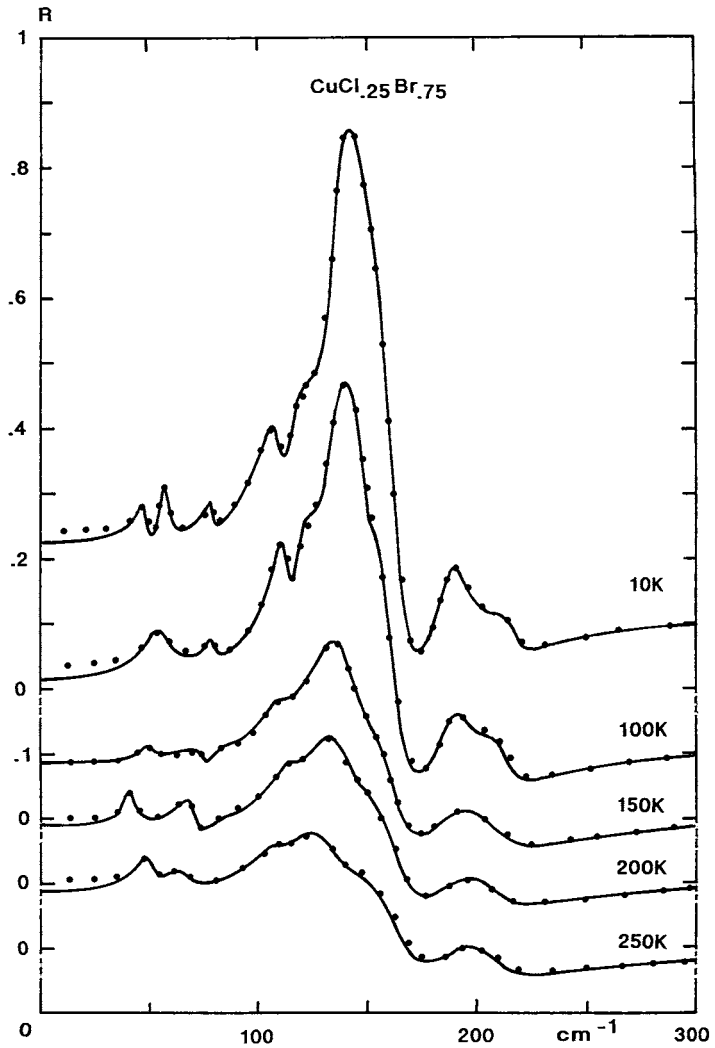

(c)

Figure 5. (Continued)

of oscillator 2 are nearly temperature independent, while those of oscillator 1 decrease with increasing temperature (figure 7(c)), with approximately the temperature frequency shift of those of the CuBr β mode (figure 2(b)) (tables 5 and 6). A similar result was observed for the TO(1) Raman line ([23], figure 3).

4.2. Discussion

The main result which arises from the analysis of the far-IR reflectivity spectra of $CuCl_{1-x}Br_x$ mixed crystals is that three polar lattice modes are active in each mixed crystal ($0 < x < 1$), at all temperatures (tables 5 and 6). However, at first sight, the far-IR reflectivity spectra of $CuCl_{1-x}Br_x$ at 10 K (figures 4 and 5) in which two reflection bands are observed between 120 and 240 cm^{-1} for $0 < x < 1$, seem in agreement with previous far-IR absorption [13, 18]

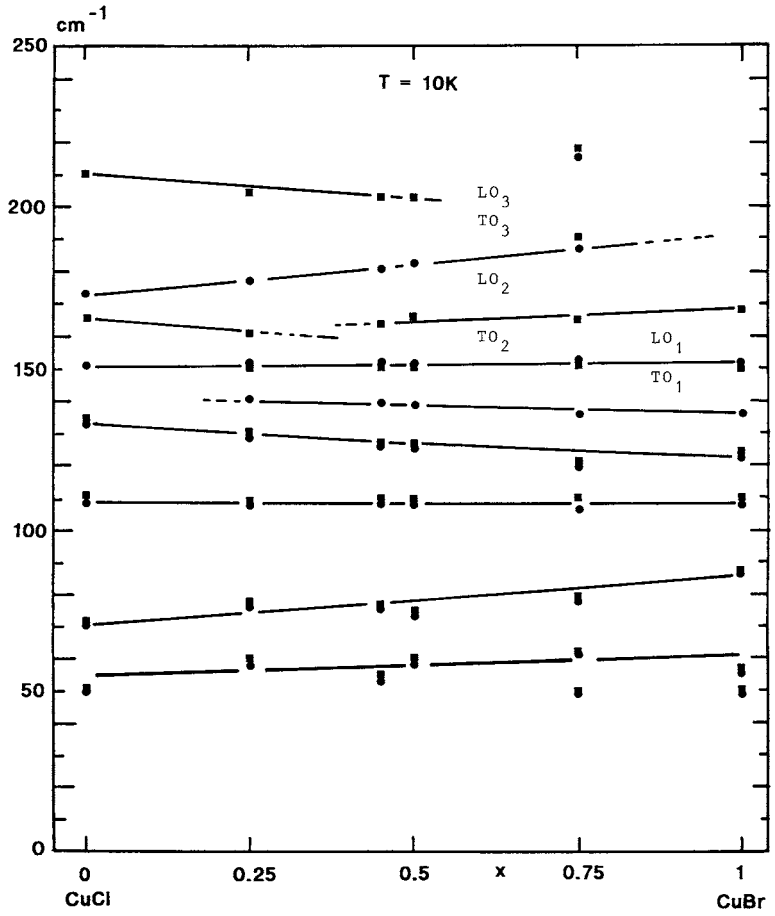

(a)

Figure 6. Concentration dependence of the TO (●) and LO (■) frequencies of the $CuCl_{1-x}Br_x$ mixed crystals: (a) at 10 K; (b) at 150 K; (c) at 250 K. The lines serve as guides to the eye.

and Raman spectra of $CuCl_{1-x}Br_x$ at 2 K [13, 18, 23], which display the activity of two polar modes in the same spectral range ([13], figure 1, [18], figure 2, and [23], figure 1).

From their far-IR absorption and Raman spectra at 4 K, Murahashi *et al* concluded that $CuCl_{1-x}Br_x$ shows a two-mode behaviour [13, 18]. They observed that the intensity of the highest-frequency mode, which emerges from the γ mode of CuCl, drops to zero with $x \rightarrow 1$. But, in contrast to the behaviour expected for a two-mode phonon branch in a solid solution, the intensity of the lowest-frequency mode, which emerges from the CuBr mode, does not drop to zero with $x \rightarrow 0$ [13, 18, 23].

The analysis of the present far-IR reflectivity spectra displays that the results reported in figure 6 are in agreement with previous far-IR and Raman spectra [13, 18, 23] only for the highest-frequency mode (oscillator 3), which is gradually reduced in intensity and disappears at high Br concentration (figure 6, tables 5 and 6) as observed previously [13, 18, 23]. This lattice mode, whose frequencies are well separated from those of oscillator 2, at every temperature (figure 7) for each studied concentration (figure 6), emerges from the γ mode of CuCl and represents the contribution of the γ CuCl mode in the mixed $CuCl_{1-x}Br_x$ crystals. Its oscillator

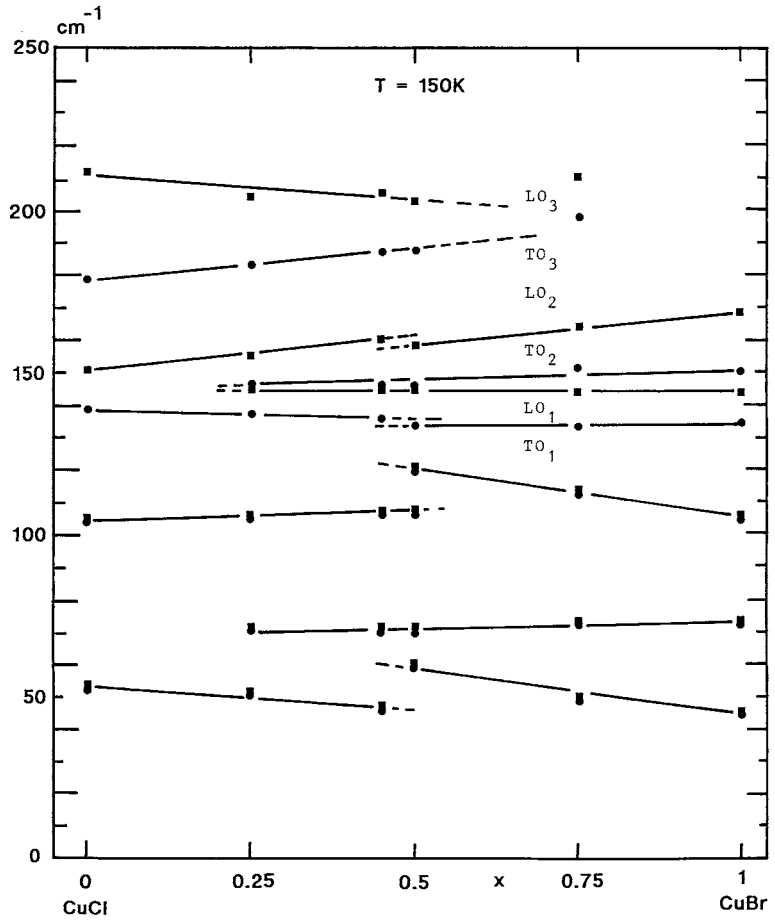

(b)

Figure 6. (Continued)

strength decreases with decreasing Cl concentration and drops to zero with $x \rightarrow 1$, at all temperatures (table 5 and 6). Our analysis, which proves the activity of two other polar lattice modes (oscillators 1 and 2) in the 130–170 cm^{-1} frequency range, excludes the possibility of a pure two-mode behaviour in the mixed $CuCl_{1-x}Br_x$ crystals, as proposed previously [13, 18].

The origin of the two lowest-frequency lattice modes (oscillators 1 and 2) is not as obvious as that of oscillator 3. However, we can obtain some indication on the origin of these modes from the analysis of the far-IR reflectivity spectra of these crystals.

(i) Figure 6 shows clearly that for high Br concentration, the lattice modes corresponding to oscillators 1 and 2 originate respectively from the β and γ modes of CuBr, at every temperature. For $x = 0.75$, the TO and LO frequencies of oscillators 1 and 2 have respectively the same temperature dependence (figure 7(c)) as those of the β and γ modes of CuBr (figure 2(b)), as well as for their oscillator strength $\Delta\varepsilon_1$ and $\Delta\varepsilon_2$, which respectively decreases and increases with increasing temperature, with $\Delta\varepsilon_1 > \Delta\varepsilon_{\beta(CuBr)}$ and $\Delta\varepsilon_2 < \Delta\varepsilon_{\gamma(CuBr)}$ at each temperature, except at 250 K where $\Delta\varepsilon_2 \approx \Delta\varepsilon_{\gamma(CuBr)}$ (tables 5 and 6). Therefore, for high Br concentration ($x > 0.75$) the contribution of CuBr

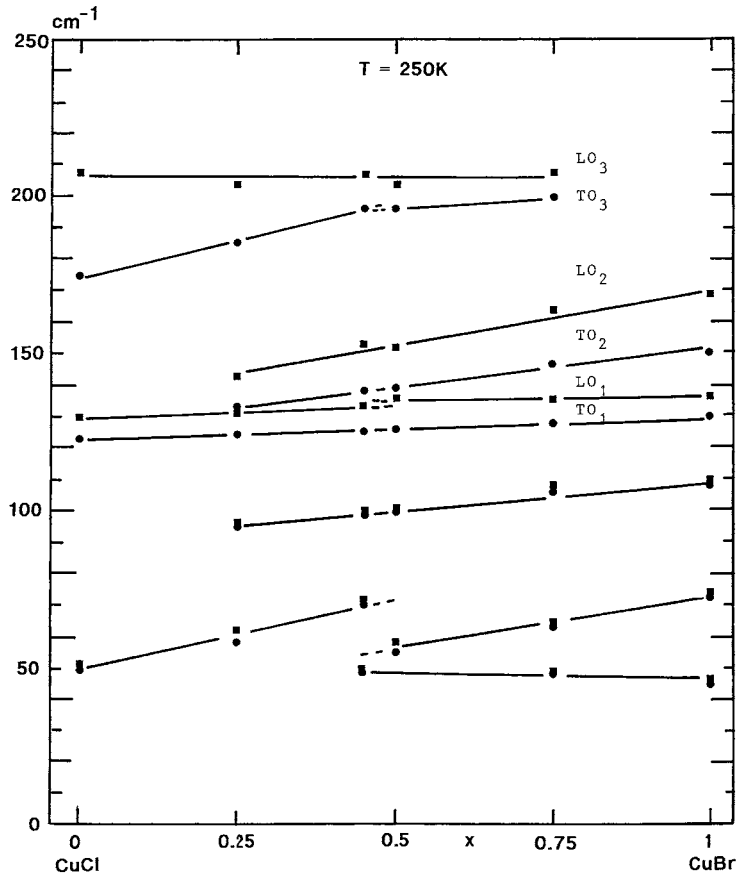

(c)

Figure 6. (Continued)

is significant: oscillators 1 and 2 represent respectively the contribution of the β and γ CuBr modes. The presence of CuCl in the crystal lattice is manifested by the activity of oscillator 3 and the modification of the oscillator strengths of the three lattice modes (tables 5 and 6).

When the Br concentration decreases below 0.75, for a given temperature the strength of both oscillators 1 and 2 increases with decreasing x, up to a maximum value observed for $0.4 < x < 0.5$, and then decreases for $x < 0.4$, with both $\Delta\varepsilon_1 > \Delta\varepsilon_{\beta(CuBr)}$ and $\Delta\varepsilon_1 > \Delta\varepsilon_{\beta(CuCl)}$, $\Delta\varepsilon_2$ keeping a value lower than $\Delta\varepsilon_{\gamma(CuBr)}$ (tables 5 and 6), at all temperatures. At the same time, we observe an important variation of the TO and LO frequencies of the two modes with temperature (figure 7, section 4.1), until for $x = 0.25$ the frequencies of the two modes (figure 7(a)) behave with temperature as those of the β mode of CuCl (figure 3). These results seem to indicate that the β CuCl mode is incorporated with either the β or the γ CuBr mode to give rise to oscillator 1 or 2, since its TO and LO frequencies change with temperature and coincide accidentally with those of the β or γ CuBr mode as seen in figure 6 and tables 1 and 2. Therefore, for $0.4 < x < 0.5$ both contributions of CuCl and CuBr are important; oscillators 1 and 2 have their strongest oscillator strength in this concentration range,

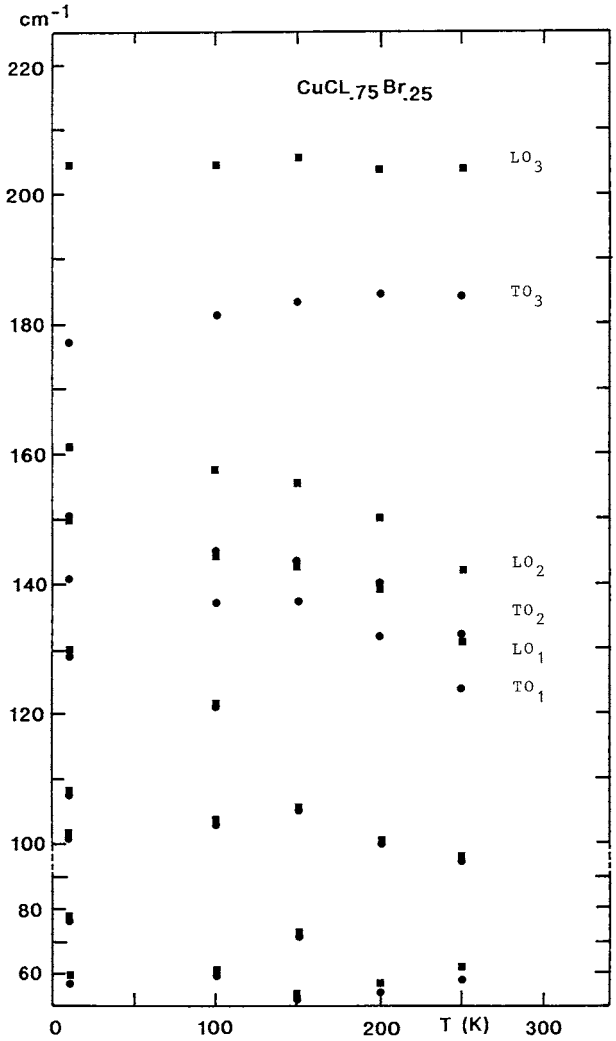

(a)

Figure 7. Temperature dependence of the TO (●) and LO (■) frequencies of the $CuCl_{1-x}Br_x$ mixed crystals: (a) for $x = 0.25$; (b) for $x = 0.5$; (c) for $x = 0.75$.

at every temperature (tables 5 and 6), while for high Cl concentration ($x < 0.4$) the contribution of CuCl is significant: $\Delta\varepsilon_1 > \Delta\varepsilon_{\beta(CuCl)}$, $\Delta\varepsilon_2$ has its lowest and $\Delta\varepsilon_3$ its highest value; oscillator 3 represents the contribution of the γ CuCl mode at all temperatures.

(ii) Let us consider the concentration dependence of the frequencies of the three lattice modes at a given temperature (figure 6). At 250 K, the frequencies LO_1 and TO_2 are distinct for $x > 0.25$; the value of their difference increases with x, from 4 cm^{-1} for $x = 0.45$ up to 11.5 cm^{-1} for $x = 0.75$ (figure 6(c)). The frequencies of the β CuCl mode have neighbouring values to those of the β CuBr mode, and are well separated from those of the γ CuBr mode (table 6, figure 6(c)). Therefore, the β mode of CuCl and that of CuBr are very close in energy, and can be incorporated to give rise to a lattice mode: oscillator 1, active

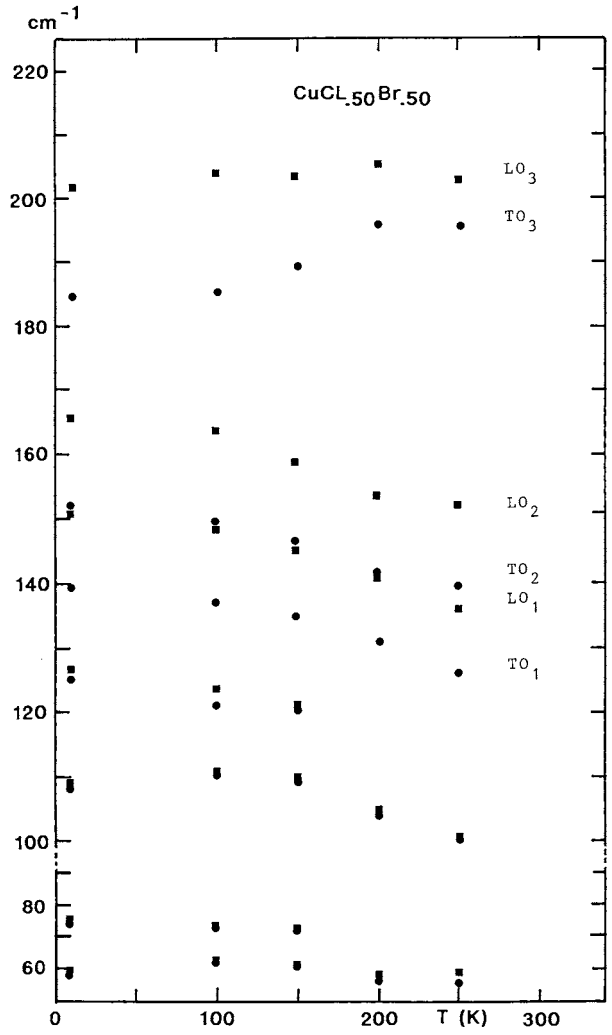

(b)

Figure 7. (Continued)

in the mixed crystal for $0 < x < 1$ (figure 6(c)). The oscillator strength of this mode is nearly constant ($\Delta\varepsilon_1 \approx 1.3$) for $0 < x < 1$, and higher than for each of the two pure compounds ($\Delta\varepsilon_\beta \approx 0.85$) (table 6). The two other lattice modes (oscillators 3 and 2) represent respectively the contribution of the γ mode of CuCl and that of CuBr. They behave with the concentration x as expected: $\Delta\varepsilon_3$ decreases while $\Delta\varepsilon_2$ increases with increasing x.

When the temperature decreases below 250 K, the LO_1 and TO_2 frequencies become nearer and the value of their difference decreases, until at 10 K it is very weak ($< 2\ \mathrm{cm}^{-1}$) at all concentrations (figures 6(a) and 6(b)); at the same time the β CuCl mode frequencies increase until at 10 K they have neighbouring values to those of both the β and γ mode of CuBr (table 5 and figure 6(a)). It is therefore difficult to assign which of the two CuBr modes is incorporated with the β CuCl mode. If one considers that at 10 K the oscillator strength of oscillator 1 is stronger than that of both CuCl and CuBr β modes (table 5), as

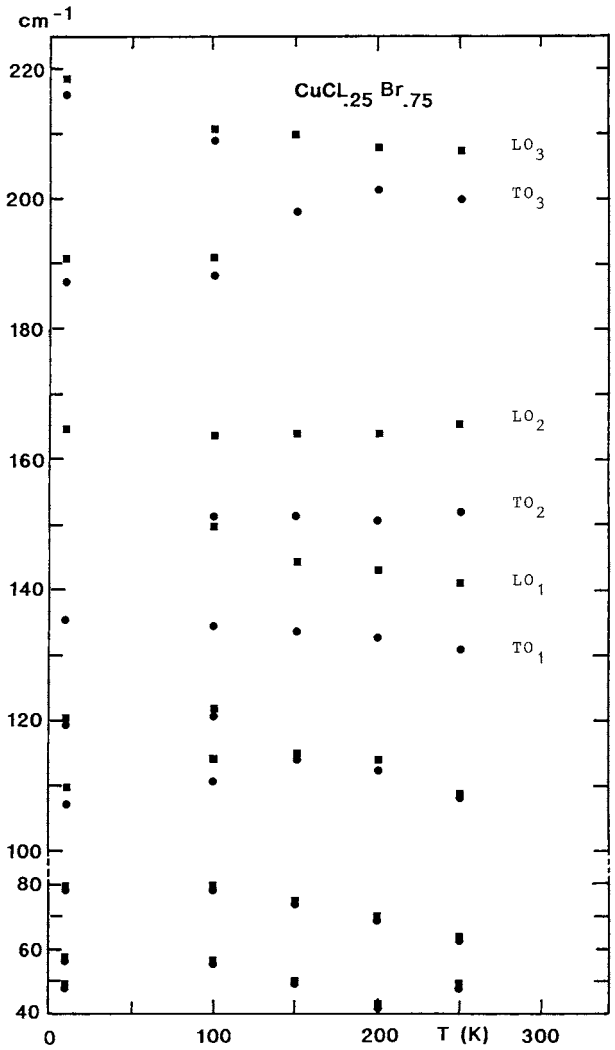

(c)

Figure 7. (Continued)

observed at every temperature, and that for a given concentration $\Delta\varepsilon_1$ decreases with increasing temperature as observed for $\Delta\varepsilon_{\beta(CuCl)}$ and $\Delta\varepsilon_{\beta(CuBr)}$, it seems probable that the β CuCl mode is incorporated with the β CuBr mode, to give rise to the lowest-frequency lattice mode (oscillator 1).

The present analysis can be compared with that of Livescu *et al* [23], which shows that three oscillators are needed to fit the experimental polariton dispersion curves of $CuCl_{1-x}Br_x$ at 11 K, while the Raman spectra at 2 K display only two pairs of TO–LO lines for $0 < x < 1$ [23]. In their analysis, the highest-frequency oscillator (labelled 2) represents the TO(γ) CuCl mode contribution as oscillator 3 in the present analysis, the two other oscillators (labelled 1 and d) represent the contribution of the TO(β) CuCl and TO CuBr modes observed in the Raman spectra ([23], figures 1 and 2). These two oscillators correspond to oscillators 1 and

2 we have assigned to the interaction of the β CuCl mode with the β CuBr mode, which depends on both concentration and temperature. These two analyses show that the peculiar behaviour of phonons in $CuCl_{1-x}Br_x$ crystals results from their structure, which is composed of tetrahedra built with Cl^- and Br^- ions, allowing the activity of both the β and γ modes of each pure compound in the mixed crystal lattice.

5. Two-phonon optical modes in CuCl, CuBr and $CuCl_{1-x}Br_x$ crystals

Several weak reflection bands are observed below 130 cm^{-1}, in the low-frequency range of the IR reflectivity spectrum of pure CuCl and CuBr crystals (figure 1), as well as in those of the $CuCl_{1-x}Br_x$ mixed crystals (figures 4 and 5), between 10 and 250 K, while no reflection band is observed in the present IR reflectivity study between 200 and 600 cm^{-1}, neither in pure or in mixed crystals (sections 3.1 and 4.1, figures 1, 4 and 5). The optical mode parameter values of the low-frequency IR active modes are reported in tables 1 and 2 for CuCl and CuBr respectively, and for mixed crystals in tables 5 and 6. The temperature dependence of the TO and LO frequencies of these modes is displayed in figures 2 and 7 respectively for pure and mixed crystals, and the concentration dependence of the TO and LO frequencies of the modes active in the mixed crystals is displayed in figure 6. Figures 1, 4 and 5 show that the low-frequency modes are more easily observed at low temperature, since their damping is strongly reduced, as for the γ and β lattice modes (tables 5 and 6).

Previous low-temperature IR absorption spectra of pure CuCl and CuBr crystals, between 2 and 80 K [3, 5], have shown that on both sides of the intense absorption peaks in the reststrahlen region about 10^{-3} times weaker side-bands are observed. These structures were interpreted as van Hove signatures in the two-phonon density of states [5]. The activity of such additional weak modes has been also observed by Raman spectroscopy on both CuCl [10, 12, 19, 20] and CuBr [16, 19, 20], as well as on $CuCl_{1-x}Br_x$ mixed crystals [21].

From tables 1, 2, 5 and 6, it can be seen that the lowest-frequency modes have a very weak TO–LO splitting, and therefore an oscillator strength weaker than the two highest-frequency β and γ lattice modes (tables 5 and 6). The low-frequency modes observed in the present work can be assigned to two-phonon processes, in both pure and mixed compounds. Such processes are allowed by selection rules [39] and therefore may be observed in the far-IR spectrum of polar semiconductors as Cu halides [3, 5, 21]. The lowest-frequency mode, whose frequencies slightly shift with the concentration from CuCl to CuBr at 10 K (figure 6(a)), can be assigned to zone boundary TA phonons, in agreement with both Raman [21] and neutron scattering measurements [29] as well as with calculated values for CuCl: TA(X) = 47.7 cm^{-1} and TA(L) = 35 cm^{-1} [35]. The second-lowest-frequency mode, whose frequencies increase by about 16 cm^{-1} with concentration, from CuCl to CuBr, can be assigned to a 2TA combination, in agreement with Raman experiments [21] as well as with calculated values for CuCl [35], but in contrast to the Raman study [21], we did not observe the splitting of these two modes at low temperature. Besides these modes, two modes are IR active between 100 and 130 cm^{-1} (tables 1, 2, 5 and 6) which were not observed in the Raman spectra [21], but in the CuCl and CuBr IR absorption spectra [5]. These modes can be assigned to LA(L) and LA(X), respectively the lowest- and the highest-frequency mode, in agreement with both the experimental neutron diffraction study of CuCl at 4 K [29] and the theoretical calculation of the frequency values at the high-symmetry points of the Brillouin zone for CuCl [35].

The intensity of the low-frequency modes is a function of the concentration x and has its highest value around an equal mixture of the two compounds (table 5). Such behaviour was observed for the low-frequency Raman lines, labelled d and α, active in the $CuCl_{1-x}Br_x$ mixed crystals [21]. We have observed in section 4.2 that the two lattice modes (oscillators 1

and 2) active in the $CuCl_{1-x}Br_x$ mixed crystals have their strongest oscillator strength in the concentration range $0.4 < x < 0.5$, at every temperature (tables 5 and 6). These results suggest that a structure with a higher statistical order exists around an equal mixture of CuCl and CuBr than for $0 < x < 0.4$ and $0.5 < x < 1$, for the $CuCl_{1-x}Br_x$ mixed crystals. Such a result was observed for $x = 0.25$ and $x = 0.75$ in the case of lead halide mixed crystals $PbCl_{2x}Br_{2(1-x)}$, i.e. when the anion sites are half-filled by each type of anion [40]. A detailed structural study of the arrangement of the Cl^- and Br^- anions building up the tetrahedra in $CuCl_{1-x}Br_x$, as a function of concentration and temperature, is highly desirable to give experimental support to the interpretation of the spectroscopic results.

6. Conclusion

In the present work we have reinvestigated the temperature dependence of the far-infrared reflectivity spectrum of CuCl and CuBr crystals, and achieved the far-infrared reflectivity spectroscopic study of $CuCl_{1-x}Br_x$ mixed crystals as a function of the concentration and temperature. We have presented and discussed here the optical-phonon anomalies of CuCl and CuBr crystals, and the peculiar behaviour of the optical-phonon spectrum in their mixed crystals $CuCl_{1-x}Br_x$. The IR reflectivity spectra were recorded with a high precision, allowing the observation of a weak inflexion in the asymmetric reflection band in the CuBr and $CuCl_{1-x}Br_x$ reflectivity spectrum.

The analysis of the experimental data, using the factorized form of the dielectric function, proves the activity of two lattice modes, not only in CuCl but also in CuBr. These modes were assigned using the off-centre model to the expected γ mode and to the additional β mode [20, 24], in agreement with previous Raman spectroscopic studies on CuCl [20, 22, 24]. We have calculated their TO and LO frequencies and their oscillator strength for both crystals, and observed that these parameters have the same temperature dependence, in CuCl as well as in CuBr. The activity of the additional β mode in CuBr, established in the present work, gives experimental support to both the off-centre model and to theoretical calculation expecting an off-centre position for Cu^+ in the CuBr crystal [34]. Therefore the off-centre model is able to explain the phonon anomaly not only in CuCl, as shown from the Raman study [20, 24], but also in CuBr.

The analysis of the far-IR reflectivity spectra of $CuCl_{1-x}Br_x$ solid solutions as a function of concentration and temperature proves the activity of three lattice modes in each $CuCl_{1-x}Br_x$ mixed crystal. We have calculated their TO and LO frequencies together with their oscillator strength. The concentration dependence of these parameters is not that characteristic of a two-mode behaviour. The anomalies observed in the spectrum are explained by the activity of the additional β mode of both CuCl and CuBr in their mixed crystals, whose interaction gives rise to the lowest-frequency lattice mode, which depends on both temperature and concentration. Such a study using far-IR reflectivity spectroscopy was never done in the past, only Raman spectroscopy has been used [13, 18, 21, 23].

Low-frequency modes, much weaker than the β and γ lattice modes, were observed below 130 cm^{-1}, in the far-IR reflectivity spectrum of both pure and mixed crystals. These modes, due to two-phonon processes, are assigned to a combination of zone boundary phonons.

Acknowledgments

The present work is dedicated to our friends Guy Morlot and Armand Hadni who were the first to investigate the far-infrared reflectivity spectra of cuprous halide crystals, down to liquid helium temperature, 35 years ago.

The authors wish to thank Dr Paul Becker and Dr Michel Certier who provided them with good quality crystals, and Dr Gérard Jeandel for the experimental facilities.

References

[1] Henninger Y, Morlot G and Hadni A 1965 *J. Physique* **26** 143
[2] Plendl J N, Hadni A, Claudel J, Henninger Y, Morlot G, Strimer P and Mansur L C 1966 *Appl. Opt.* **5** 397
[3] Hadni A, Bréhat F, Claudel J and Strimer P 1968 *J. Chem. Phys.* **49** 471
[4] Ikezawa M 1973 *J. Phys. Soc. Japan* **35** 309
[5] Mayurama M, Namba T and Ikezawa M 1978 *J. Phys. Soc. Japan* **44** 1231
[6] Namba T, Hachisu K and Ikezawa M 1981 *J. Phys. Soc. Japan* **50** 1579
[7] Iwaza S and Burstein E 1965 *J. Physique* **26** 614
[8] Prévot B, Carabatos C and Leroy M 1972 *C. R. Acad. Sci. Paris* **274** 707
[9] Nusimovici M A and Meskaoui A 1972 *Phys. Status Solidi* b **52** K69
[10] Kaminov I P and Turner E H 1972 *Phys. Rev.* B **5** 1564
[11] Hanson R C, Hallberg J R and Schwab C 1972 *Appl. Phys. Lett.* **21** 490
[12] Prévot B and Sieskind M 1973 *Phys. Status Solidi* b **59** 133
[13] Murahashi T, Koda T, Oka Y and Kushida T 1973 *Solid State Commun.* **13** 307
[14] Potts J E, Hanson R C, Walker C T and Schwab C 1973 *Solid State Commun.* **13** 389
[15] Potts J E, Hanson R C, Walker C T and Schwab C 1974 *Phys. Rev.* B **9** 2711
[16] Turner E H, Kaminov I P and Schwab C 1974 *Phys. Rev.* B **9** 2524
[17] Shand M L, Hochheimer H D, Krauzman M, Potts J E, Hanson R C and Walker C T 1976 *Phys. Rev.* B **14** 4637
[18] Murahashi T and Koda T 1976 *J. Phys. Soc. Japan* **40** 747
[19] Fukumoto T, Nakashima S, Tabuchi K and Mitsuishi A 1976 *Phys. Status Solidi* b **73** 341
[20] Vardeny Z and Brafman O 1979 *Phys. Rev.* B **19** 3276
[21] Vardeny Z and Brafman O 1979 *Phys. Rev.* B **19** 3290
[22] Vardeny Z and Brafman O 1980 *Phys. Rev.* B **21** 2585
[23] Livescu G, Vardeny Z and Brafman O 1981 *Phys. Rev.* B **24** 1952
[24] Livescu G and Brafman O 1986 *Phys. Rev.* B **34** 4255
[25] Carabatos C, Hennion B, Kunc K, Moussa F and Schwab C 1971 *Phys. Rev. Lett.* **26** 770
[26] Prévot B, Carabatos C, Schwab C, Hennion B and Moussa F 1973 *Solid State Commun.* **13** 1725
[27] Hennion B, Moussa F, Prévot B, Carabatos C and Schwab C 1972 *Phys. Rev. Lett.* **28** 964
[28] Hoshino S, Fujii Y, Harada J and Axe J D 1976 *J. Phys. Soc. Japan* **41** 965
[29] Prévot B, Hennion B and Dorner B 1977 *J. Phys. C: Solid State Phys.* **10** 3999
[30] Hennion B, Prévot B, Krauzman M, Pick R M and Dorner B 1979 *J. Phys. C: Solid State Phys.* **12** 1609
[31] Sakata M, Hoshino S and Harada J 1974 *Acta Crystallogr.* A **30** 655
[32] Schreurs J, Mueller M H and Schwartz L H 1976 *Acta Crystallogr.* A **32** 618
[33] Miyake S and Hoshino S 1958 *Rev. Mod. Phys.* **30** 172
[34] Wei Su-Huai, Zhang S B and Zunger A 1993 *Phys. Rev. Lett.* **70** 1639
[35] Wang Cheng-Zhang, Yu R and Krakauer H 1994 *Phys. Rev. Lett.* **72** 368
[36] Wyncke B, Strimer P, El Sherif M, Bréhat F and Jacquot C 1983 *Revue Phys. Appl.* **18** 355
[37] Gervais F 1983 *Infrared and Millimeter Waves* vol 8, ed K J Button (New York: Academic) ch 7
[38] Plendl J N and Mansur L C 1972 *Appl. Opt.* **11** 1194
[39] Ziman J M 1965 *Principles of the Theory of Solids* (Cambridge: Cambridge University Press)
[40] Carabatos-Nédelec C and Lumbreras M 1965 *J. Raman Spectrosc.* **21** 291